Table S1. Summary of bond lengths and bond angles of SnPi-P and SnPi-B, as extracted from the PDF analysis.

Bond lengths

Connectivity	SnPi-P (Å)	SnPi-B (Å)
P1-O1	1.575	1.666
Sn1-O1	2.064	2.031
O1-O2	2.495	2.441
Sn1-P1	3.317	3.341
Sn1-O2	3.632	3.696
Sn1-P2	5.096	5.011
Sn1-Sn2	5.627	5.627

Bond angles

Connectivity	SnPi-P	SnPi-B
<O1P1O4	113.87°	122.21°
<P1O2Sn2	130.97°	129.02°
<P1O4P2	180°	180°

Comment: SnPi-P has the O-P-O bond tilted/squeezed by almost 8° more towards the P-O-P bond compared to SnPi-B, as shown in **Figure 3b1-3c1**. As a consequence, the P-O bond is shorter for SnPi-P than SnPi-B. On the contrary, the P-O-Sn bond of SnPi-P is much more open by almost 2°, compared to SnPi-B with longer Sn-O bond. The mesoporous architecture of SnPi-P has the critical effect towards the bond lengths and bond angles among the constituent atoms to achieve the more energetically favourable structure with the same crystal system.

Table S2. Comparison of surface areas and pore diameters of various mesoporous tin phosphate materials in the presence of different structure directing agents.

Entry	Template (Structure directing agent)	Surface Area ($m^2 \cdot g^{-1}$)	Pore diameter (nm)	Mesostructures	Crystallinity	Ref.
1	Cetyl trimethyl ammonium bromide (CTAB)	76	2.3	Hexagonal (*p6mm*)	Crystalline	R1
2	Cetyl trimethyl ammonium bromide (CTAB)	230	2.9	Hexagonal (*p6mm*)	Amorphous	R2
3	Tetradecyl trimethyl ammonium bromide (TTAB)	425	2.0	Cubic (*Im3m*)	Amorphous	R3
4	Tetradecyl trimethyl ammonium bromide (TTAB)	109	1.7	Disordered	Crystalline	R4
5	Sodium dodecyl sulfate (SDS)	200	3.0	Disordered	Amorphous	R5
6	Pluronic P123	122	5.2	Disordered	Amorphous	R6
7	Pluronic F127	310	7.4	Hexagonal (*p6mm*)	Nanocrystalline	This Work

Figure S1

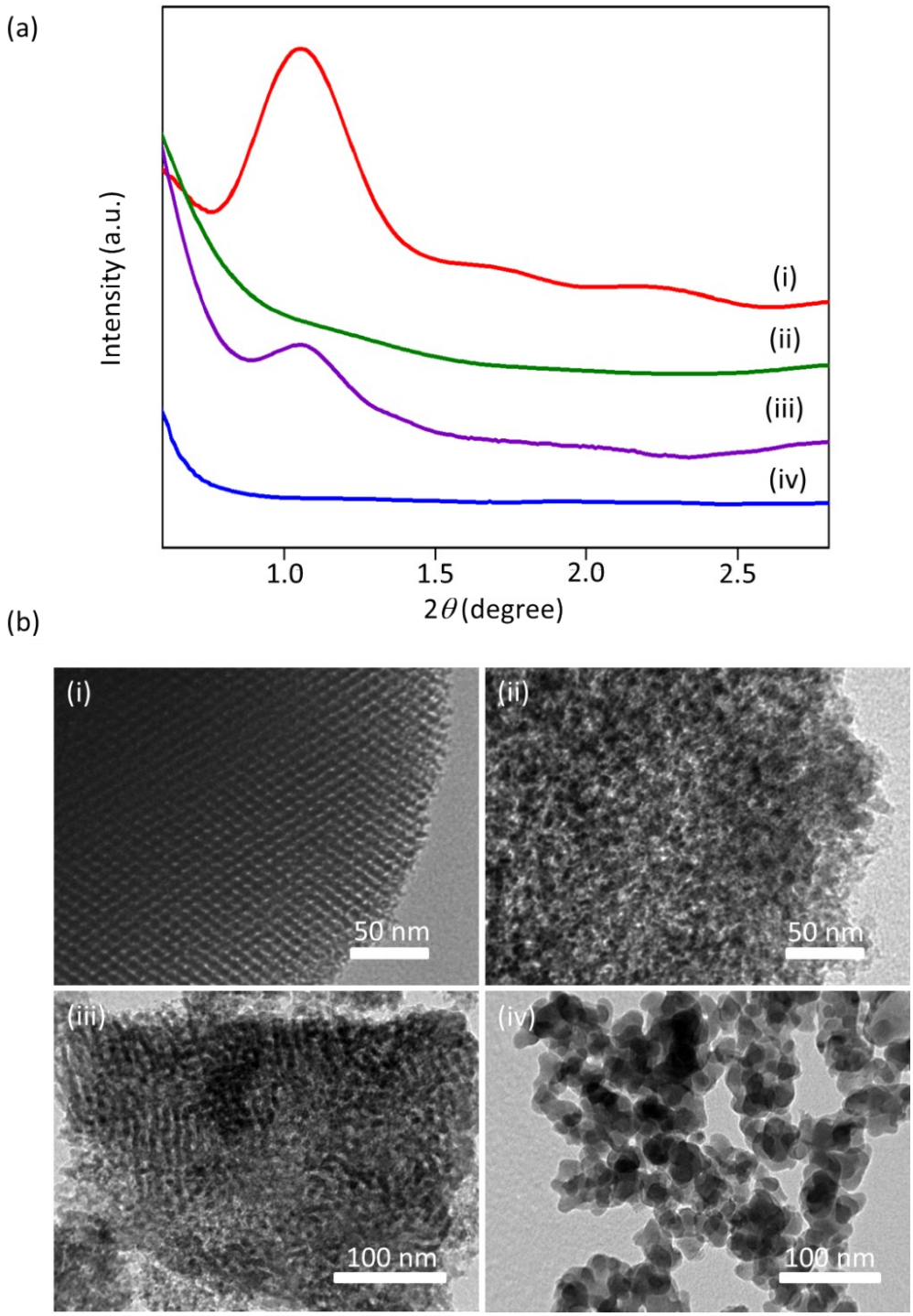

Figure S1.(a) Small-angle XRD patterns of SnPi materials under different controlled conditions: (i) synthesized in the presence of HF, followed by a two-step calcination (the typical condition, SnPi-P), (ii) synthesized in the presence of HF, followed by direct calcination, (iii) synthesized in the absence of HF, followed by a two-step calcination, and (iv) synthesized without a surfactant, followed by a two-step calcination (SnPi-B). (b) Corresponding TEM images of (i), (ii), (iii), and (iv).

Figure S2

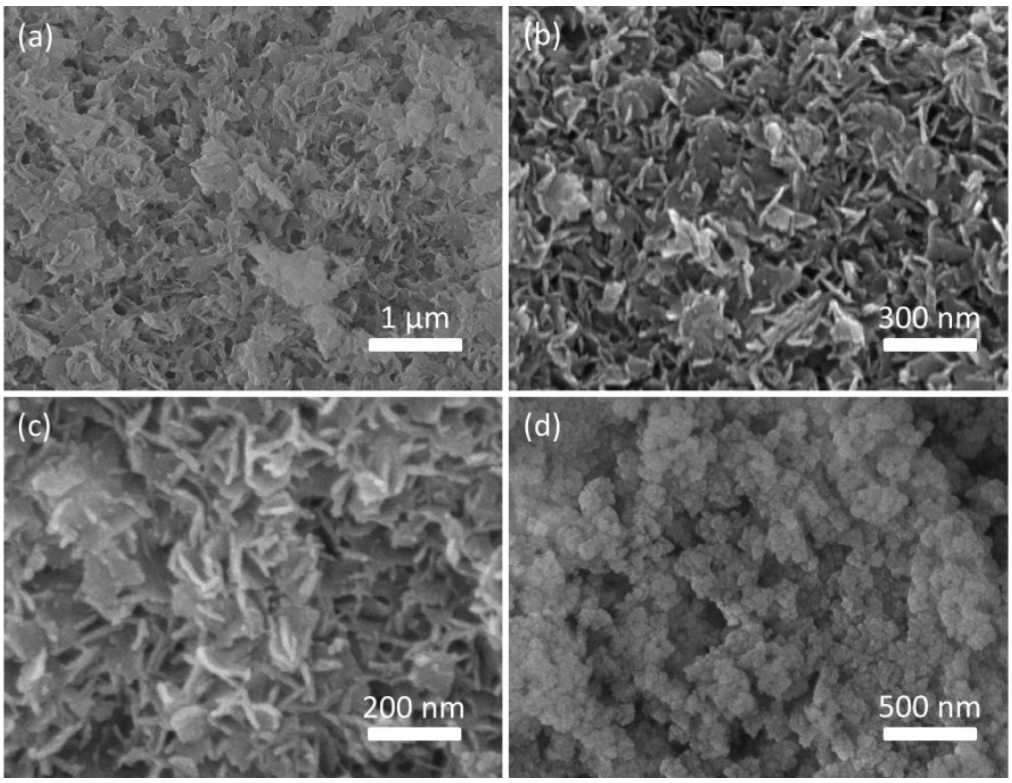

Figure S2. SEM images of (a) SnPi-A, (b) SnPi-C, (c) SnPi-P, and (d) SnPi-B.

Figure S3

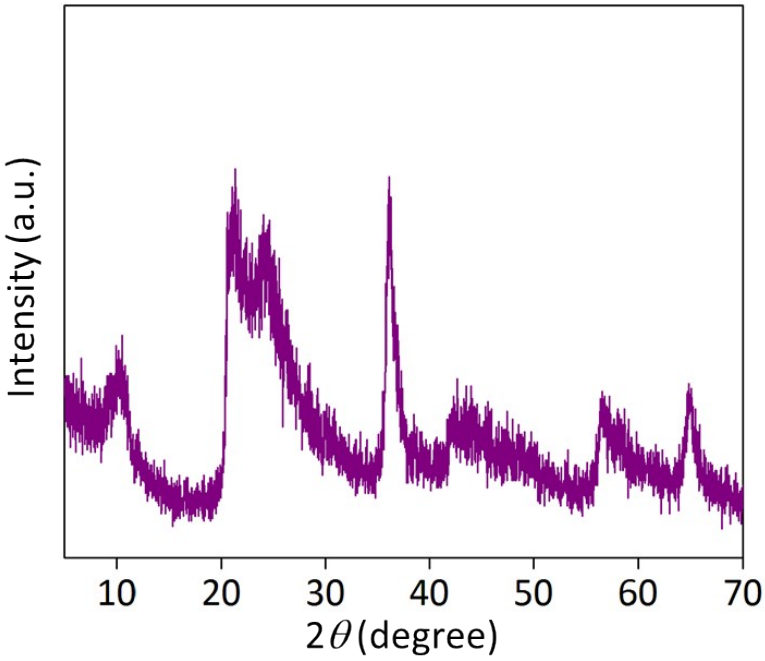

Figure S3. Wide-angle X-ray diffraction pattern of the SnPi-A.

Figure S4

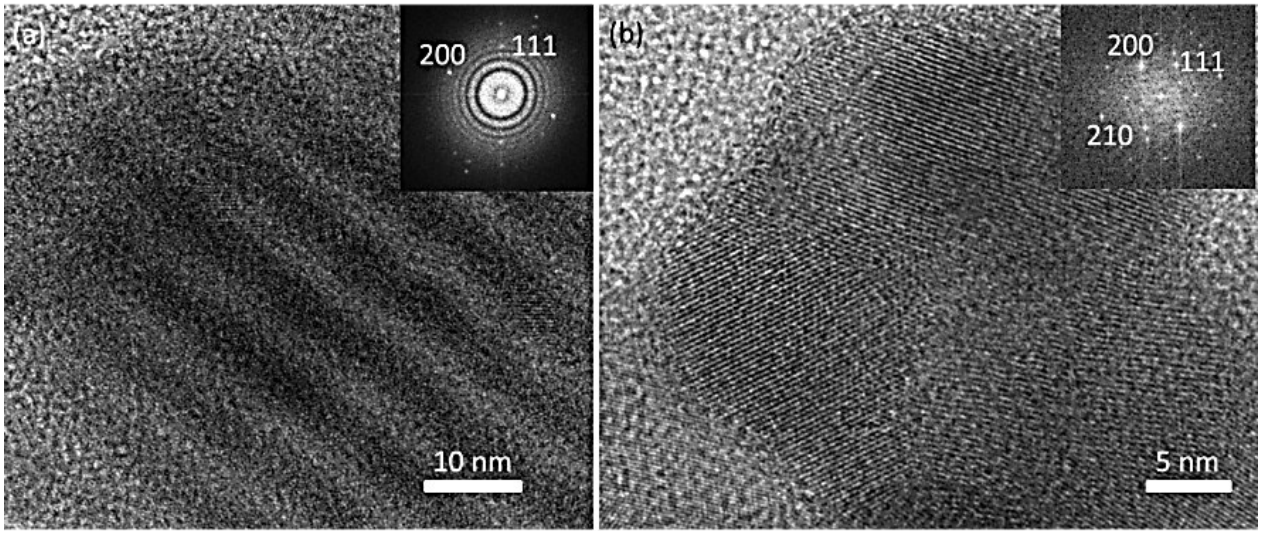

Figure S4. HR-TEM images of (a) SnPi-P showing the mesoporous channels with crystalline pore walls (inset of panel 'a' shows the corresponding FFT pattern) and (b) SnPi-B showing a crystalline particle with a large grain boundary.

Figure S5

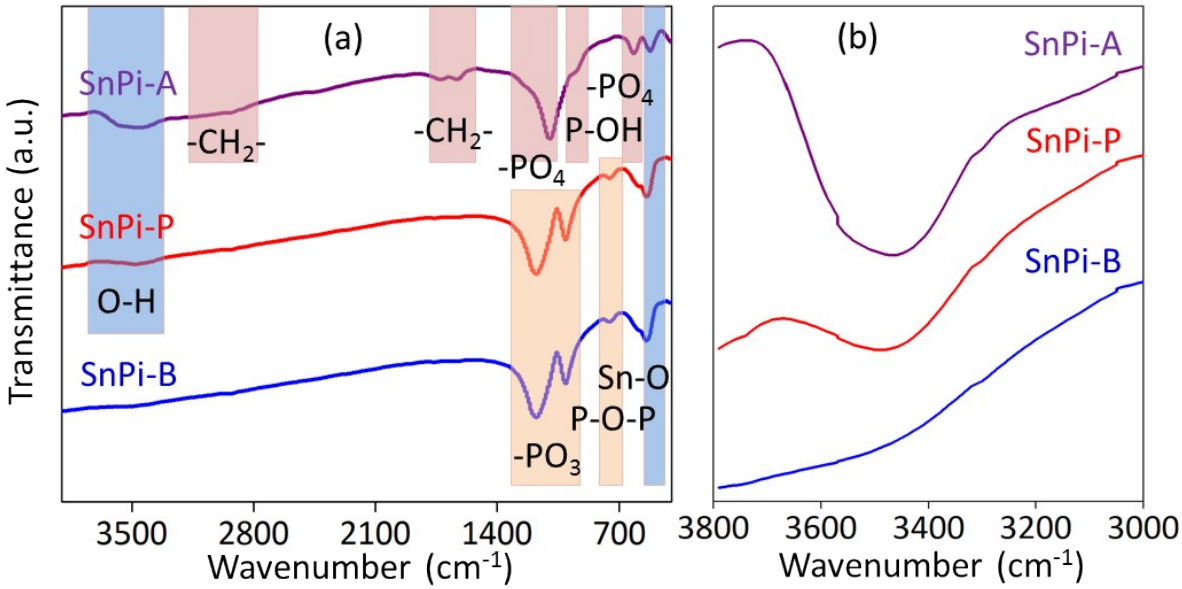

Figure S5. (a) FT-IR spectra of as-prepared SnPi (SnPi-A) and mesoporous SnPi (SnPi-P), and bulk SnPi (SnPi-B); (b) Enlarged spectra of the O-H stretching vibration region.

Comment: In the FT-IR spectrum of SnPi-A, the two peaks at around 520 cm^{-1} and 625 cm^{-1} can be assigned to Sn-O stretching and $-PO_4$ bending vibrations. The peak at 940 cm^{-1} is due to the stretching vibration of the free/uncoordinated P-OH in the framework. The characteristic band at around 1098 cm^{-1} is due to the $-PO_4$ stretching vibration. The broad band from 3200-3700 cm^{-1} is due to the stretching vibration of O-H, from the surface adsorbed water molecules, free P-OH, orF127 template present in the as-prepared SnPi-A sample.[R7] The excess broadening of the O-H stretching vibration clearly indicates the presence of an H-bonding interaction between F127 and tin phosphate precursor in the as-prepared SnPi-A (**Figure S5b**). The extra peaks for the as-prepared SnPi-A sample are at 1590 cm^{-1}, 2926 cm^{-1}, and 3014 cm^{-1}, which are related to $-CH_2-$ bending, and to $-CH_2-$ symmetric and asymmetric stretching vibrations, respectively.[R8]These extra peaks are due to the presence of F127. In the case of SnPi-P after removal of the F127 template, the peak at 750 cm^{-1} is due the vibration mode of the P-O-P bond, a signature peak of the SnP_2O_7 structure. The characteristic frequencies at about 1030 cm^{-1} and 1174 cm^{-1} are assigned to symmetric and asymmetric vibration peaks for $-PO_3$ in the SnP_2O_7 structure.[R9]The peak at 3475 cm^{-1} for SnPi-P corresponds to O-H stretching vibration, indicating the presence of O-H group. In contrast, SnPi-B has no peaks for this region. This free O-H group generated from uncoordinated P-OH group or Sn-O-H bond formation.

Figure S6

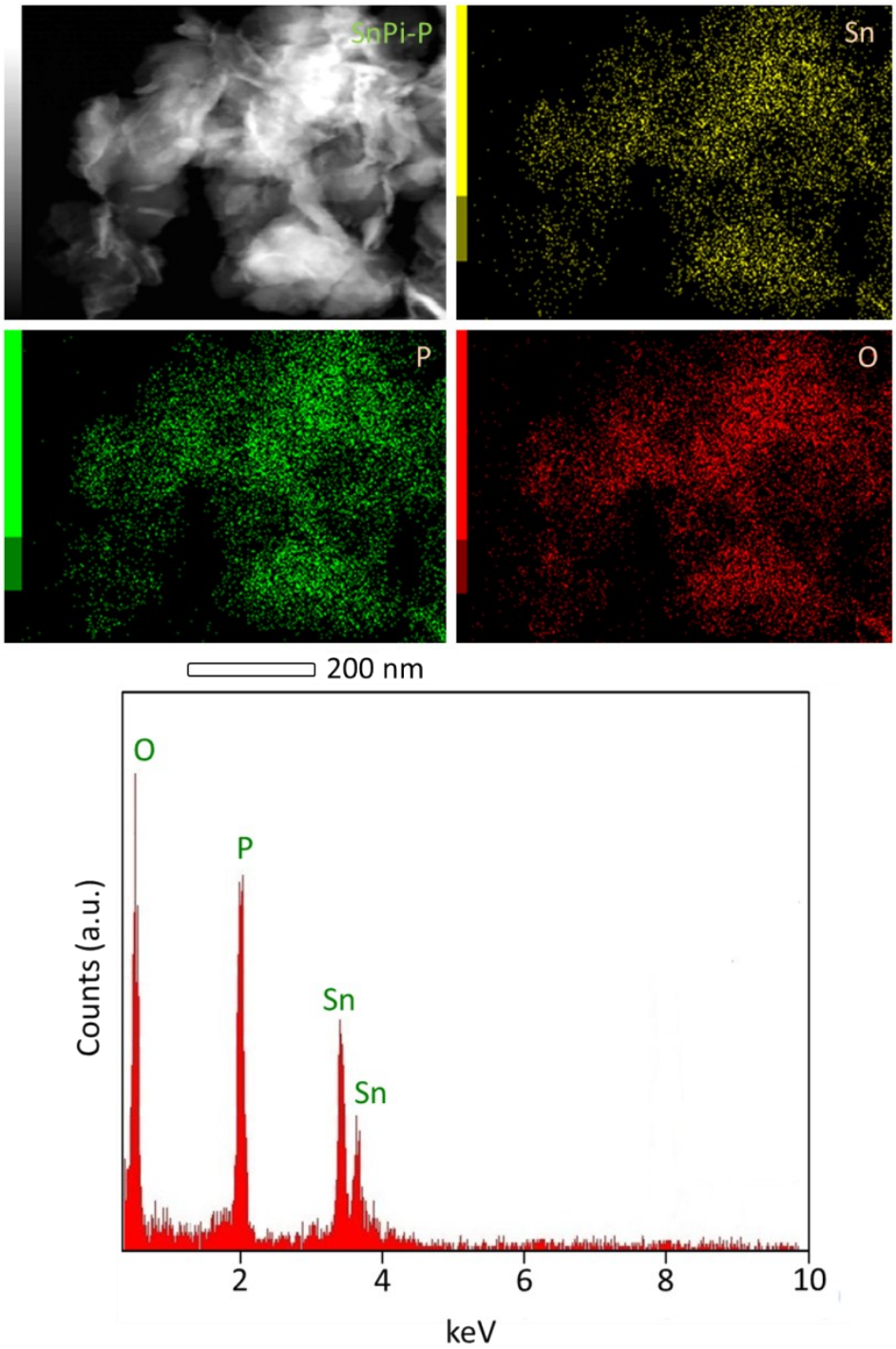

Figure S6. Elemental mapping of SnPi-P (top), and energy dispersive spectroscopy (EDS) spectrum (bottom).

Figure S7

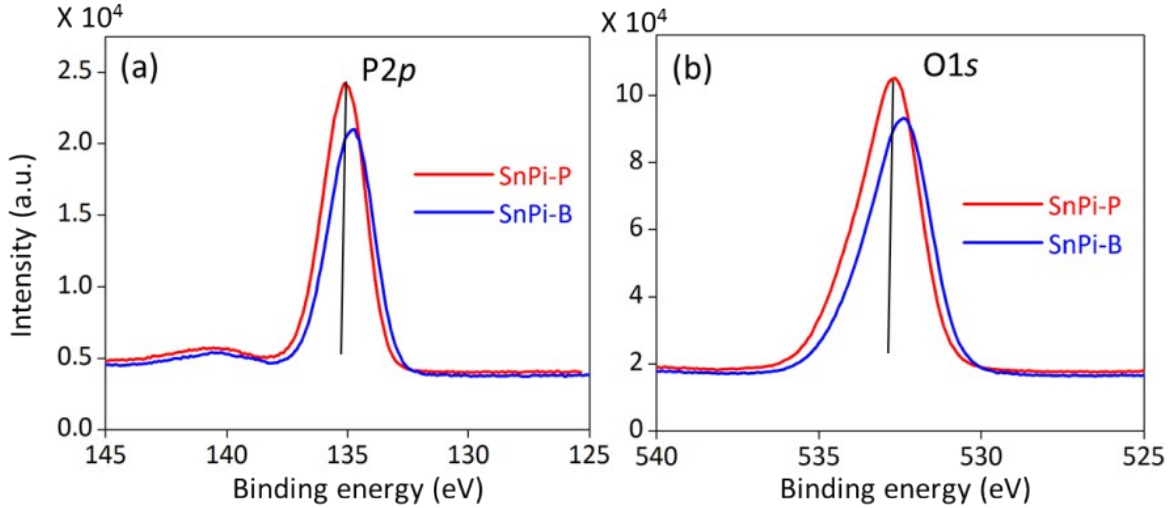

Figure S7. XPS spectra of (a) P 2*p* and (b) O 1*s* peaks of SnPi-P and SnPi-B.

Figure S8

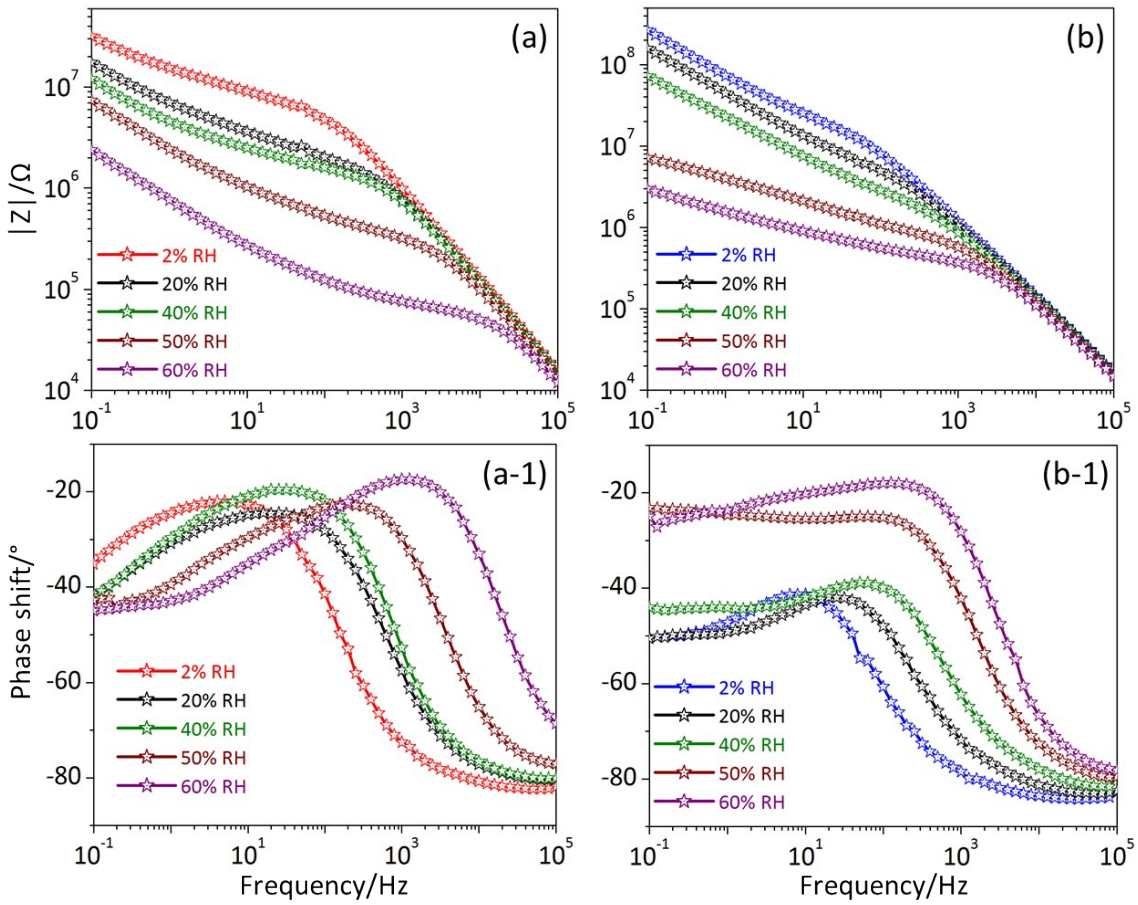

Figure S8. Bode plots of (a, a-1) SnPi-P and (b, b-1) SnPi-B at 2%, 20%, 40%, 50% and 60% RH and room temperature (293 K).

Table S3. Comparison of proton (H^+) conductivity of our mesoporous SnPi (SnPi-P) with various state-of-art metal phosphates.

Entry	Sample	Conductivity ($S \cdot cm^{-1}$)	Measurement temperature (K)	Relative humidity (% RH)	References
1	Titanium pyrophosphate (TiP_2O_7)	1.0×10^{-6}	573	-	R10
2	Bismuth phosphate ($Bi_2P_4O_{13}$)	2.0×10^{-8}	523	5	R11
3	Cesium dihydrogen phosphate (CsH_2PO_4)	1.8×10^{-6}	423	15	R12
4	Neodymium phosphate ($NdPO_4$)	0.8×10^{-4}	423	15	R12
5	Zirconium dihydrogen phosphate (α-$Zr(HPO_4)_2$)	1.0×10^{-4}	373	97	R13
6	Lanthanum phosphate ($LaPO_4$)	9.7×10^{-9}	700	-	R14
7	Tin pyrophosphate (SnP_2O_7)	8.0×10^{-9}	673	-	R15
8	Mesoporous Zirconium pyrophosphate (ZrP_2O_7)	4.0×10^{-7}	293	20	R16
9	Cerium pyrophosphate (CeP_2O_7)	3.6×10^{-6}	673	6	R17
10	Calcium Phosphate ($Ca_5(PO_4)_3(OH)$)	7.0×10^{-6}	1073	-	R18
11	Tin pyrophosphate (SnP_2O_7)	1×10^{-5}	523	-	R19
12	Mesoporous SnPi (SnPi-P)	5.5×10^{-7}	293	60	This Work
13	Nonporous SnPi (SnPi-B)	8.6×10^{-8}	293	60	This Work

Table S4. Comparison of electrochemical performances of our mesoporous SnPi (SnPi-P) with various state-of-art metal phosphates as anode materials in LIB.

Entry	Samples	Cycle numbers	1st discharge capacity ($mAh\ g^{-1}$)	Current density ($mA\ g^{-1}$)	Potential Window (V)	Capacity retention (%)	Refs
1	$Sn_2P_2O_7$ nanodisks	220	900	350	0~1.2	93	R20
2	Porous $Sn_2P_2O_7$	50	880	72	0.001~2.5	56	R21
3	Mesoporous $Sn_2P_2O_7$	30	1080	72	0~2.5	81	R22
4	VPO_4 nanoparticles	30	548	20	0.01~3.0	42	R23
5	$FePO_4$ nanoparticles	30	609	61	0~2.4	80	R24
6	Mesoporous SnPi (SnPi-P)	20	750	72	0~2.5	92	This Work

References

R1 E. Kim, D. Son, T. G. Kim, J. Cho, B. Park, K. S. Ryu and S. H. Chang, *Angew. Chem.*, 2004, **116**, 6113.

R2 N. K. Mal, S. Ichikawa and M. Fujiwara, *Chem. Commun.*, 2002, 112.

R3 C. Serre, A. Auroux, A. Gervasini, M. Hervieu and G. Ferey, *Angew. Chem.*, 2002, **114**, 1664.

R4 E. Kim, M. G. Kim, Y. Kim and J. Cho, *Electrochem. Solid-State Lett.*, 2005, **8**, A452.

R5 H. Kim, G. S. Park, E. Kim, J. Kim, S. G. Doo and J. Cho, *J. Electrochem. Soc.*, 2006, **153**, A1633.

R6 B. Tian, X. Liu, B. Tu, C. Yu, J. Fan, L. Wang, S. Xie, G. D. Stucky and D. Zhao, *Nat. Mater.*, 2003, **2**, 159.

R7 (a) A. B. Goncalves, A. S. Mangrich and A. J. G. Zarbin, *Synthetic Metals*, 2000, **114**, 119; (b) A. I. Bortun, S. A. Khainakov, L. N. Bortun, E. Jaimez, J. R. Garcia and A. Clearfield, *Mater. Res. Bull.*, 1999, **34**, 921.

R8 (a) Y. Shen, M. Nishida, W. Kanematsu and T. Hibino, *J. Mater. Chem.*, 2011, **21**, 663; (b) Z. Wu, C. Guo, S. Liang, H. Zhang, L. Wang, H. Sun and B. Yang, *J. Mater. Chem.*, 2012, **22**, 18596.

R9 X. Wu, A. Verma and K. Scott, *Fuel Cells*, 2008, **8**, 453.

R10 V. Nalini, M. H. Sorby, K. Amezawa, R. Haugsrud, H. Fjellva and T. Norbyz, *J. Am. Ceram. Soc.*, **2011**, *94*, 1514.

R11 Y. Huang, E. Christensen, Q. Shuai and Q. Li, *Int. J. Hydrogen Energy*, 2016, 1.

R12 T. Anfimova, A. H. Jensen, E. Christensen, J. O. Jensen,N. J. Bjerrum and Q. Li, *J. Electrochem. Soc.*, 2015, **162**, F436.

R13 G. Alberti, M. Casciola, U. Costantino, A. Peraio and T. Rega, *J. Mater. Chem.*, 1995, **5**, 1809.

R14 G. Harley, R. Yu and L. C. De Jonghe, *Solid State Ion.*, 2007, **178**, 769.

R15 S. Tao, *Solid State Ion.*, 2009, **180**, 148.

R16 G. Alberti, M. Casciola, S. Cavalaglio and R. Vivani, *Solid State Ion.*,1999,**125**, 91.

R17 B. Singh, H. N. Im, J. Y. Park and S. J. Song, *J. Electrochem. Soc.*, 2012, **159**, F819.

R18 D. Liu, K. Savino and M. Z. Yates, *Adv. Funct. Mater.*, 2009, **19**, 3941.

R19 X. Xu, S. Tao, P. Wormalda and J. T. S. Irvine, *J. Mater. Chem.*, 2010, **20**, 7827.

R20 S. Lee and J. Cho, *Chem. Commun.*, 2010, **46**, 2444.

R21 J. G. Lee, D. Son, C. Kim and B. Park, *J. Power Sources*,2007, **172**, 908.

R22 E. Kim, D. Son, T. G. Kim, J. Cho, B. Park, K. S. Ryu and S. H. Chang, *Angew. Chem., Int. Ed.*, 2004, **43**, 5987.

R23 Y. Zhang, X. J. Zhang, Q. Tang, D. H. Wu and Z. Zhou, *J. Alloys Compd.*, 2012, **522**, 167.

R24 D. Son, E. Kim, T. G. Kim, M. G. Kim, J. Cho and B. Park, *Appl. Phys. Lett.*, 2004, **85**, 5875.